SLAC-PUB-16472

Title: Three-Dimensional Charge Density Wave Order in $YBa_2Cu_3O_{6.67}$ at High Magnetic Fields

Authors: S. Gerber[1¶], H. Jang[2¶], H. Nojiri[3], S. Matsuzawa[3], H. Yasumura[3], D. A. Bonn[4,5], R. Liang[4,5], W. N. Hardy[4,5], Z. Islam[6], A. Mehta[2], S. Song[7], M. Sikorski[7], D. Stefanescu[7], Y. Feng[7], S. A. Kivelson[8], T. P. Devereaux[1], Z.-X. Shen[1,8], C.-C. Kao[9], W.-S. Lee[1*], D. Zhu[7*], J.-S. Lee[2*]

Affiliations:

[1]*Stanford Institute for Materials and Energy Science, SLAC National Accelerator Laboratory and Stanford University, Menlo Park, California 94025, USA*

[2]*Stanford Synchrotron Radiation Lightsource, SLAC National Accelerator Laboratory, Menlo Park, California 94025, USA*

[3]*Institute for Materials Research, Tohoku University, Katahira 2-1-1, Sendai, 980-8577, Japan*

[4]*Department of Physics & Astronomy, University of British Columbia, Vancouver, British Columbia, Canada V6T 1Z1*

[5]*Canadian Institute for Advanced Research, Toronto, Ontario, Canada M5G 1Z8*

[6]*The Advanced Photon Source, Argonne National Laboratory, Argonne, Illinois 60439, USA*

[7]*Linac Coherent Light Source, SLAC National Accelerator Laboratory, Menlo Park, California 94025, USA*

[8]*Geballe Laboratory for Advanced Materials, Departments of Physics and Applied Physics, Stanford University, Stanford, California 94305, USA*

This material is based upon work supported by the U.S. Department of Energy, Office of Science, Office of Basic Energy Sciences, Division of Materials Sciences and Engineering, under Contract No. DE-AC02-76SF00515.

[9]*SLAC National Accelerator Laboratory, Menlo Park, California 94025, USA*

[¶]These authors contributed equally to this work.

[*]Correspondence to: dlzhu@slac.stanford.edu, leews@stanford.edu, jslee@slac.stanford.edu

Abstract: Charge density wave (CDW) correlations have been shown to universally exist in cuprate superconductors. However, their nature at high fields inferred from nuclear magnetic resonance is distinct from that measured by x-ray scattering at zero and low fields. Here we combine a pulsed magnet with an x-ray free electron laser to characterize the CDW in $YBa_2Cu_3O_{6.67}$ via x-ray scattering in fields up to 28 Tesla. While the zero-field CDW order, which develops below $T \sim 150$ K, is essentially two-dimensional, at lower temperature and beyond 15 Tesla, another three-dimensionally ordered CDW emerges. The field-induced CDW appears around the zero-field superconducting transition temperature; in contrast, the incommensurate in-plane ordering vector is field-independent. This implies that the two forms of CDW and high-temperature superconductivity are intimately linked.

Main Text: The universal existence of charge density wave (CDW) correlations in superconducting cuprates (*1-12*) raises profound questions regarding the role of charge order – is it competing or more intimately intertwined with high-temperature superconductivity (HTSC) (*13-16*)? Uncovering the evolution of CDW order upon suppression of HTSC by an external magnetic field provides valuable insight into these issues. One of the most studied cuprate superconductors, $YBa_2Cu_3O_{6+\delta}$, has become a model material for the study of CDW phenomena in cuprates. Largely two-dimensional incommensurate CDW order with moderate correlation length has recently been found to coexist with HTSC using x-ray scattering measurements (*7, 8, 17, 18*). The temperature and magnetic field dependencies up to $\mu_0 H$ = 17 T indicate a competition between CDW order and HTSC (*8, 17*). However, both nuclear magnetic resonance (NMR) (*6, 19*) and Hall coefficient measurements (*20*) suggest that there is a distinct, more ordered CDW phase at higher fields and lower temperatures, with an NMR signature that is different than the NMR broadening (*21*) that correlates with the zero-field CDW. The existence of a phase transition or sharp crossover to a state with a distinct field-induced form of density wave order is also supported by ultrasonic measurements (*22*). However, there is a discrepancy between NMR (*19*) and ultrasonic measurements (*22*) regarding the onset field of this new state, and neither reveal the structure of the CDW at high fields. This calls for high-field x-ray scattering measurements of the CDW phenomenology in superconducting cuprates, which, however, is extremely challenging for existing techniques, especially because the scattering signal is so weak.

To gain insight into this critical question one needs to introduce a different experimental approach. Here, we perform x-ray scattering at an x-ray free electron laser (FEL) in the presence of pulsed high magnetic fields. The high brilliance of the x-ray FEL (*23*) enables the

measurement of the weak CDW scattering signal with a single x-ray pulse (~50 femtosecond) at the apex of a millisecond magnetic field pulse (*24*). This approach provides us with the opportunity to probe the CDW signal in $YBa_2Cu_3O_{6+\delta}$ at magnetic fields beyond 17 T, thereby entering a field range comparable to that used in NMR (*6, 19, 21*), Hall coefficient (*20*) and ultrasonic measurements (*22*).

Figure 1A shows a schematic of how the two pulsed sources – the magnet and the x-ray FEL – were synchronized to study the CDW in detwinned, underdoped $YBa_2Cu_3O_{6.67}$ (YBCO) with ortho-VIII oxygen order (*24*). To monitor the field dependence of the CDW, an area detector was used to capture a cut of the *kl*-plane in reciprocal space. The full view of the zero-field diffraction pattern in the vicinity of the CDW position at the zero-field superconducting transition temperature, $T_c(H = 0) = 67$ K, is shown in Fig. 1B. In this geometry, we observe CDW features centered near (0, 2-*q*, ±½) with an incommensuration $q \sim 0.318$ (*7, 8, 17, 18*). The detected diffraction pattern of the CDW shows that the correlation along the crystallographic *c*-axis is very weak, resulting in a rod-like shape along the *l*-direction. Moreover, we also measured the temperature dependence of the zero-field CDW (Fig. 1C and Ref. [*24*]), reproducing earlier reports that the CDW signal is maximal at T_c and suppressed for $T < T_c$ (*7, 8, 17, 18*), which indicates a competition between CDW order and HTSC.

We first discuss the temperature dependence of the CDW at $\mu_0 H = 20$ T. Figure 2A shows the (0, 2-*q*, *l*) CDW signal at both 0 and 20 T. There is no field-induced change of the CDW at T_c, which is consistent with earlier results (*8*). With decreasing temperature ($T < T_c$) the CDW signal becomes sharper along the *k*-direction and more intense than at zero field. This indicates that, as the magnetic field suppresses superconductivity, the CDW order is enhanced (Fig. 2B). Surprisingly, as shown in the 2D difference map $I_{20T} - I_{0T}$ (lower panels of Fig. 2A) the field-

induced enhancement is most dramatic at $l \sim 1$, rather than at $l \sim ½$ where the zero-field CDW signal is maximal (*7, 8, 17, 18*). This observation indicates that a different kind of CDW correlation emerges around $T_c(0)$ − well below the zero-field CDW onset temperature (Fig. 1C). As shown in Fig. 2C, the temperature dependence of the field-induced CDW is consistent with that of the CDW signatures inferred from NMR measurements (*6*), implying that both share the same origin.

Next we explore the field-induced enhancement of CDW order at $T = 10$ K. Figure 3A shows the diffraction patterns (upper panels) at $\mu_0 H = 0 – 25$ T. The lower panels depict the projected intensities at both $l \sim ½$ and $l \sim 1$, *i.e.*, integrated over the ranges of l indicated on the right. Up to $\mu_0 H = 15$ T the intensities of the CDW order at both $l \sim ½$ and $l \sim 1$ are similar. Above 15 T, however, the intensity at (0, 2-q, ~1) continues to grow strongly, while it saturates at (0, 2-q, ~½) (Fig. 3B). This was confirmed in an equivalent CDW region (0, 2+q, 1) (Fig. 4 and Ref. [*24*]), where we were able to follow the enhancement of CDW intensity at $l \sim 1$ up to our maximum field, $\mu_0 H = 28$ T. Furthermore, the in-plane correlation lengths ξ_k at $l \sim ½$ and $l \sim 1$ start to diverge from each other at $\mu_0 H \sim 15$ T (Fig. 3C), suggestive of a transition; ξ_k at $l \sim 1$ increases for $\mu_0 H > 15$ T, while ξ_k at $l \sim ½$ saturates or is slightly suppressed. We note that, as discussed in (*24*), the estimated correlation length at the highest magnetic fields may be limited by the instrument resolution. Nevertheless, the distinct field-dependence of the CDW intensity and the correlation length confirm that the CDW order at $l \sim 1$ is different from that at $l \sim ½$, and that both CDW orders coexist at high magnetic fields. In particular, the onset of the field-induced CDW ($l \sim 1$) above 15 T is consistent with NMR results in which the line-splitting signature of CDW order is absent at low fields (*6, 19*) and the ultrasonic measurements (*22*). Unfortunately, because of the relatively coarse field interval in Fig. 3, it is difficult to precisely determine the

value of the onset field (shaded area in Fig. 3, B and C), and or to distinguish whether the field-induced CDW emerges in a phase-transition or a crossover.

Data shown in Fig. 3 motivate scrutiny of the field-induced CDW in the l ~ 1 region at the highest accessible magnetic field of 28 T. Given our experimental configuration (*24*), a larger l-range is accessible near l = 1 by monitoring the equivalent CDW reflection near (0, 2+q, l), rather than near (0, 2-q, ~1). As shown in Figs. 4, A and B, the CDW diffraction pattern at 28 T becomes sharper not only along the k-direction (Fig. 3C), but also along the l-direction (perpendicular to the CuO_2 planes). This indicates that CDW correlations along the c-axis are enhanced, i.e. ξ_l = 34(4) and 50(2) Å at 20 and 28 T, respectively; concomitant with roughly a three-fold increase of the peak height. Even though these values of ξ_l are lower bounds, as they have not been corrected for the instrument resolution (*24*), they are significantly larger than that of the zero-field CDW (ξ_l ~ 7 Å, Ref. [*8*]), indicating the field-induced CDW at l = 1 is much more correlated in all three dimensions than the zero-field CDW. Furthermore, as shown in Figs. 4, C and D, the CDW peak positions are identical at 20 and 28 T. There has been speculation that the in-plane component of the CDW Q-vector may shift and lock-in to a commensurate value at high magnetic fields (*25*). However, within our experimental resolution the field-induced in-plane components of the Q-vector [h = 0.00(1), k = 0.318(10)] are identical to that of the zero-field CDW.

We note that a field-induced spin density wave (SDW) has been observed in $La_{2-x}Sr_xCuO_4$ at weaker fields ~6 T, which is also peaked at integer l due to an alignment of SDW patches, associated with the vortex cores (*26*). However, the emergence of field-induced CDW order at l = 1 is unlikely to be caused by the alignment of CDW regions that are associated with vortices (*2*). This is because at magnetic fields beyond 20 T, the distance between vortices, if still present,

would be less than ~100 Å in the CuO_2 plane (*27*), which is already smaller than the in-plane CDW correlation length at these field strengths (Fig. 3C).

Now we discuss implications of the observed field-induced three-dimensional CDW at l = 1. First, its emergence at high fields and low temperatures implies a boundary that separates the phase diagram into different CDW regions, as also suggested by ultrasonic (*22*) and NMR measurements (*19*). Second, given that a field-dependence of the CDW order is only observed below $T_c(0)$ (Fig. 2), we infer that the enhancement is related to the suppression of superconductivity. Thus, the growth of the CDW peak intensity in fields up to 28 T indicates that superconducting correlations exist beyond the upper critical field that was deduced from transport measurements (*28, 29*). Third, our observations shed light on quantum oscillation results, which have been interpreted as evidence for the existence of small electron pockets in the "nodal" region of the Brillouin zone (*4, 5, 30*). It is plausible that the Fermi surface is reconstructed by the stronger field-induced CDW at l = 1, rather than the shorter-range correlated one at l ~ ½ (*31*). Finally, we remark that the relation between the zero-field and field-induced CDW is puzzling. On the one hand, they seem unrelated as they exhibit distinct temperature and field dependences, as well as a different ordering perpendicular to the CuO_2 planes. On the other hand they must be somehow related, since they feature the same in-plane CDW incommensuration q. Thus, our results reveal a rich CDW phenomenology in cuprates, which is not a simple competition with HTSC.

References and Notes:

1. J. M. Tranquada, B. J. Sternlieb, J. D. Axe, Y. Nakamura, S. Uchida, *Nature* **375**, 561 – 563 (1995).
2. J. E. Hoffman *et al.*, *Science* **295**, 466 – 469 (2002).
3. C. Howald, H. Eisaki, N. Kaneko, A. Kapitulnik, *Proc. Natl. Acad. Sci. USA* **100**, 9705 – 9709 (2003).
4. N. Doiron-Leyraud *et al.*, *Nature* **447**, 565 – 568 (2007).
5. D. LeBoeuf *et al.*, *Nature* **450**, 533 – 536 (2007).
6. T. Wu *et al.*, *Nature* **477**, 191 – 194 (2011).
7. G. Ghiringhelli *et al.*, *Science* **337**, 821 – 825 (2012).
8. J. Chang *et al.*, *Nat. Phys.* **8**, 871 – 876 (2012).
9. R. Comin *et al.*, *Science* **343**, 390 – 392 (2014).
10. E. H. da Silva Neto *et al.*, *Science* **343**, 393 – 396 (2014).
11. W. Tabis *et al.*, *Nat. Commun.* **5**, 5875 (2014).
12. E. H. da Silva Neto *et al.*, *Science* **347**, 282 – 285 (2015).
13. E. Fradkin, S. A. Kivelson, *Nat. Phys.* **8**, 864 – 866 (2012).
14. H.-D. Chen, O. Vafek, A. Yazdani, S.-C. Zhang, *Phys. Rev. Lett.* **93**, 187002 (2004).
15. P. A. Lee, *Phys. Rev. X* **4**, 031017 (2014).
16. D. F. Agterberg, J. Garaud, *Phys. Rev. B* **91**, 104512 (2015).
17. S. Blanco-Canosa *et al.*, *Phys. Rev. Lett.* **110**, 187001 (2013).
18. E. Blackburn *et al.*, *Phys. Rev. Lett.* **110**, 137004 (2013).
19. T. Wu *et al.*, *Nat. Commun.* **4**, 2113 (2013).
20. D. LeBoeuf *et al.*, *Phys. Rev. B* **83**, 054506 (2011).

21. T. Wu *et al.*, *Nat. Commun.* **6**, 6438 (2015).

22. D. LeBoeuf *et al.*, *Nat. Phys.* **9**, 79 – 83 (2013).

23. P. Emma *et al.*, *Nat. Photon.* **4**, 641 – 647 (2010).

24. Materials and methods are available as supplementary materials on *Science* Online.

25. E. M. Forgan *et al.*, (2015), http://arxiv.org/abs/1504.01585.

26. B. Lake *et al.*, *Nat. Mater.* **4**, 658 – 662 (2005).

27. N. Galvan Leos *et al.*, *J. Phys. Soc. Jpn.* **84**, 044709 (2015).

28. G. Grissonnanche *et al.*, *Nat. Commun.* **5**, 3280 (2014).

29. G. Grissonnanche *et al.*, (2015), http://arxiv.org/abs/1503.07572.

30. S. E. Sebastian, N. Harrison, G. G. Lonzarich, *Rep. Prog. Phys.* **75**, 102501 (2012).

31. S. E. Sebastian *et al.*, *Nature* **511**, 61 – 64 (2014).

Acknowledgments: We thank J. Hastings, J. Defever, D. Damiani, G. Curie and V. Borzenet for technical assistance in developing the scattering setup. Discussions with C. Mielke are acknowledged. This work was supported by the Department of Energy (DOE), Office of Science, Basic Energy Sciences, Materials Sciences and Engineering Division, under contract DE-AC02-76SF00515. X-ray FEL studies were carried out at the Linac Coherent Light Source, a Directorate of SLAC and an Office of Science User Facility operated for the U.S. DOE, Office of Science by Stanford University. Soft and hard x-ray scattering studies were carried out at the Stanford Synchrotron Radiation Lightsource, a Directorate of SLAC and an Office of Science User Facility operated for the U.S. DOE, Office of Science by Stanford University. Hard x-ray scattering studies were also conducted at the Advanced Photon Source, supported by the U.S. DOE, Office of Science, Office of Basic Energy Sciences under Contract No. DE-AC02-

06CH11357. S.G. acknowledges partial support by the Swiss National Science Foundation under Fellowship No. P2EZP2_148737. H.N. acknowledges the support by KAKENHI 23224009, ICC-IMR and MD-program. Materials development was supported by the Natural Sciences and Engineering Research Council, and by the Canadian Institute for Advanced Research.

Supplementary Materials

www.sciencemag.org

Materials and Methods

Figs. S1 to S5

References (32-35)

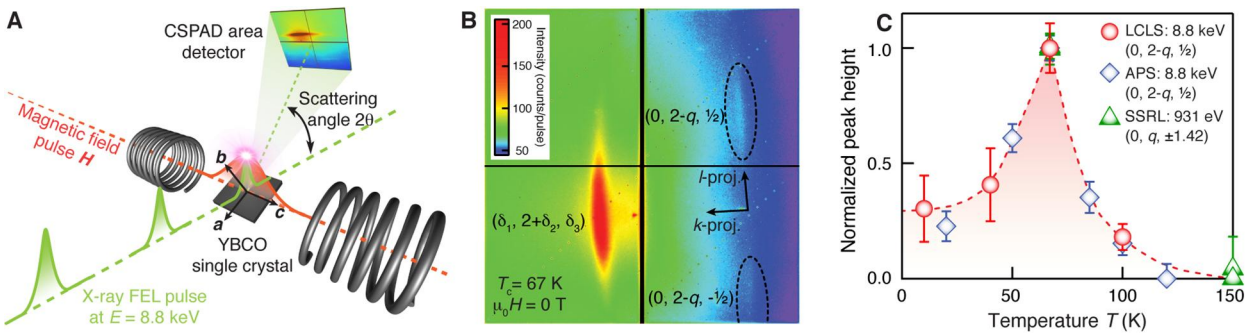

Fig. 1. Experimental setup and zero-field characterization. (**A**) The millisecond pulsed magnetic field and femtosecond x-ray FEL pulses are synchronized to obtain a diffraction pattern from the YBCO single crystal at the maximum magnetic field. The diffraction pattern was recorded using a 2D pixel array detector. (**B**) Zero-field diffraction pattern showing the (0, 2-*q*, ±½) CDW peaks and the tail of the (0, 2, 0) Bragg peak (δ_1= -0.118, δ_2 = 0.001, δ_3 = 0.021). The sample rotation angle was optimized for the CDW position and not for the (0, 2, 0) Bragg peak (*24*). (**C**) The temperature dependence of the CDW peak height near (0, 2-*q*, ½) measured at the x-ray FEL is shown with red colored symbols. We have also taken data at synchrotron lightsources using hard (blue symbols) and soft (green symbols) x-rays (*24*), which are shown for comparison. The dashed line is a guide-to-the-eye and the error bars denote 1 standard deviation (s.d.) as obtained from the peak fitting.

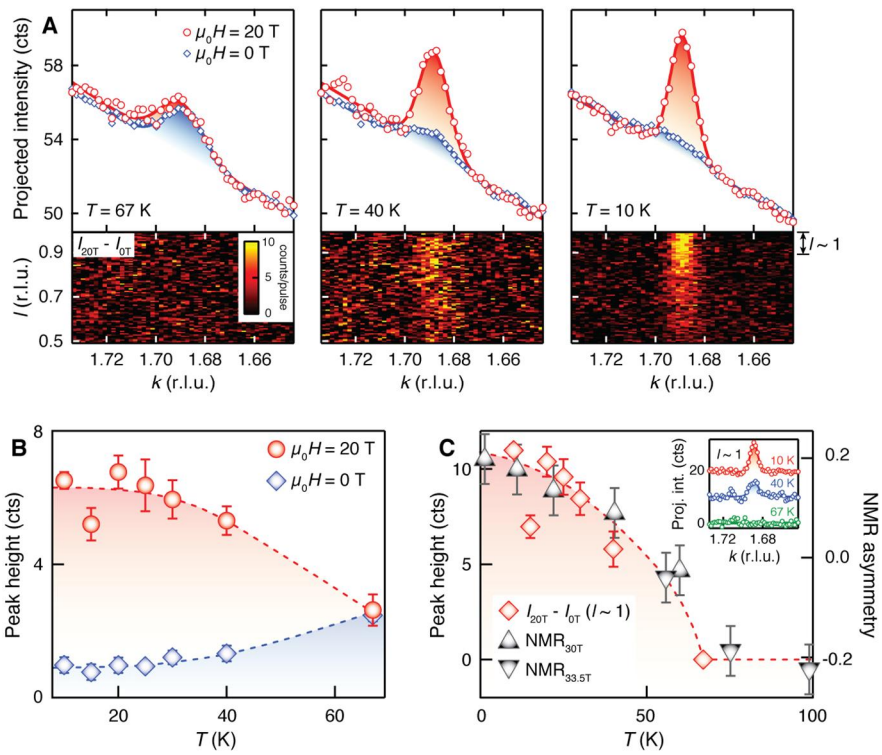

Fig. 2. Temperature dependence of the CDW order at μ_0H = 20 T. (**A**) The upper and lower panels show the evolution of the projected (0, 2-*q*, ½) CDW peak profile along the *k*-direction and the difference map of the diffraction pattern between μ_0H = 0 and 20 T, respectively, at representative temperatures of *T* = 67, 40, and 10 K. Positions are given in reciprocal lattice units (r.l.u.). Solid lines are Gaussian fits to the data with a 2nd order polynomial background. (**B**) *T*-dependence of the peak height from the projected CDW profiles at 0 and 20 T. (**C**) Peak height of the projected CDW profiles near *l* ~ 1 as a function of temperature. The projected CDW profiles (inset, traces offset by 10 cts) are obtained from the 2D difference map by integrating near *l* ~ 1, as indicated in (**A**). As a comparison NMR data taken from Ref. (*6*) are superimposed. Dashed lines are guides-to-the-eye. Error bars correspond to 1 s.d.

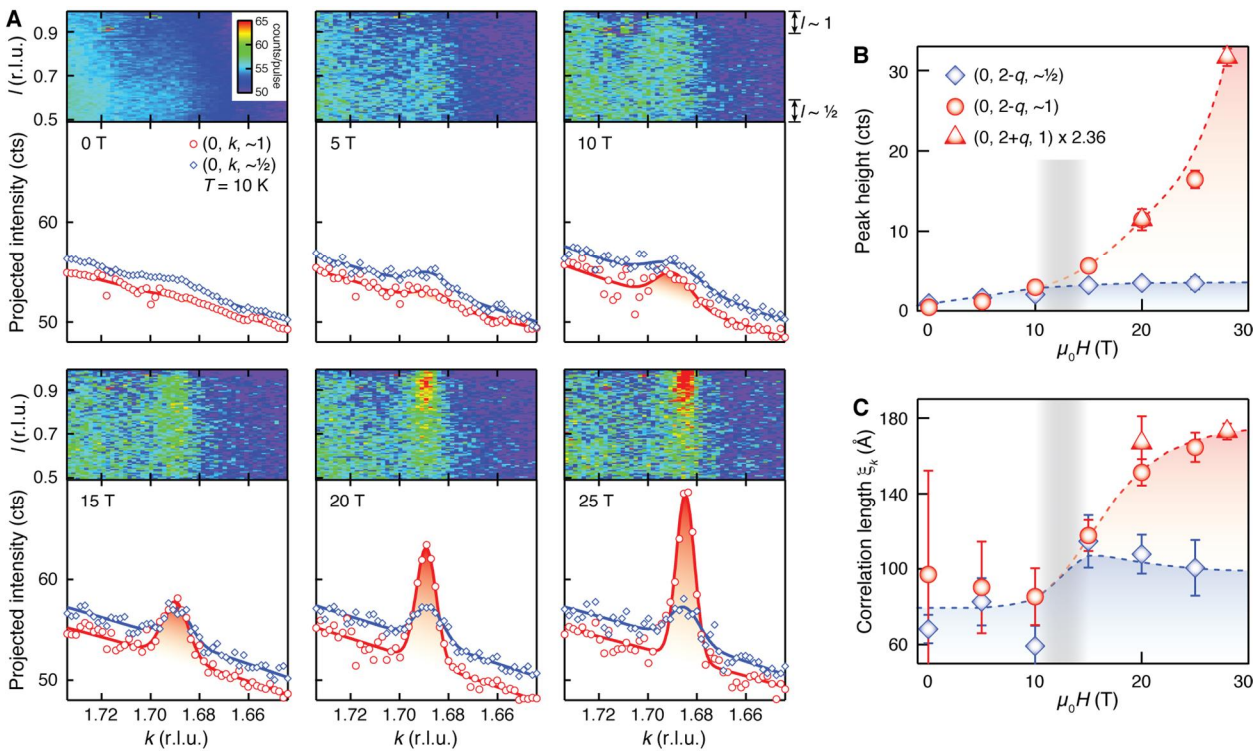

Fig. 3. Field dependence of the CDW order at *T* = 10 K. (**A**) CDW diffraction pattern (upper panels) and projected CDW peak profiles (lower panels) near l ~ ½ and l ~ 1, obtained by integration of the signal in the windows indicated on the image, in the field range $\mu_0 H$ = 0 – 25 T. Features due to ice condensation on the sample surface, which do not overlap with the CDW signal, were subtracted from the diffraction patterns (*24*). Solid lines are Gaussian fits to the data with a 2nd order polynomial background. (**B**) Peak height of the projected CDW profile near l ~ ½ and l ~ 1 as a function of H. Data taken in an equivalent CDW region (0, 2+q, 1), shown in Fig. 4, are superimposed by normalizing the values at 20 T. (**C**) H-dependence of the in-plane correlation length $\xi_k = 1/\sigma_k$ deduced from Gaussian fits (σ_k is the Gaussian standard deviation) to the projected CDW profile shown in (**A**) as well as Fig. 4C. Values of ξ_k have not been corrected for the instrument resolution and, therefore, represent lower bounds. The grey shaded area denotes the onset region of the l ~ 1 CDW component and dashed lines are guides-to-the-eye. Error bars correspond to 1 s.d.

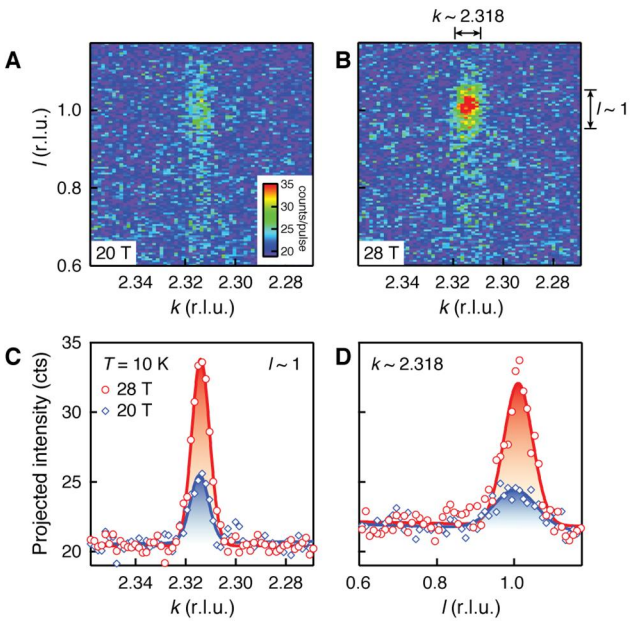

Fig. 4. Three-dimensional CDW order at $\mu_0 H$ > 20 T. (**A** and **B**) CDW diffraction pattern near (0, 2+*q*, *l*) at $\mu_0 H$ = 20 and 28 T. (**C** and **D**) Projected CDW peak profiles along the *k*- and *l*-direction within the regions indicated in (**B**). Gaussian fits to the data with a linear background (solid lines) and taking into account the measurement accuracy, reveal that the field-induced CDW peak is centered at *k* = 2.318(10) and *l* = 1.00(2).